Supporting Information

Nanoscale control of rewriteable doping patterns in pristine graphene/boron nitride heterostructures

Jairo Velasco Jr.[1,5,†], Long Ju[1,†], Dillon Wong[1,†], Salman Kahn[1], Juwon Lee[1], Hsin-Zon Tsai[1], Chad Germany[1], Sebastian Wickenburg[1], Jiong Lu[1,‡,Δ] , Takashi Taniguchi[4], Kenji Watanabe[4], Alex Zettl[1,2,3], Feng Wang[1,2,3] and Michael F. Crommie[1,2,3,*]

[1]*Department of Physics, University of California, Berkeley, California 94720, USA*

[2]*Materials Sciences Division, Lawrence Berkeley National Laboratory, Berkeley, California 94720, USA*

[3]*Kavli Energy NanoSciences Institute at the University of California, Berkeley and the Lawrence Berkeley National Laboratory, Berkeley, California 94720, USA*

[4]*National Institute for Materials Science, 1-1 Namiki, Tsukuba, 305-0044, Japan*

[5] *Department of Physics, University of California, Santa Cruz, California 95064, USA*

[†] *These authors contribute equally to this manuscript.*

[*] *Email:crommie@berkeley.edu*

[‡] Present address: *Department of Chemistry, National University of Singapore, 3 Science Drive 3, Singapore 117543,Singapore*

[Δ] Present address: *Centre for Advanced 2D Materials and Graphene Research Centre, National University of Singapore, 6 Science Drive 2, Singapore 117546*

Table of Contents:

1. Determination of $\tilde{V}_g$ for light–induced doping

Light-induced doping modifies both the global charge density and the local charge density profile. To focus on the latter, we carefully choose $\tilde{V}_g$ to eliminate the former. This is done in the following manner: First, dI/dV spectra are measured at the same location in all maps in order to track the charge neutrality point (CNP) after each light exposure treatment; next, this information is used to tune the gate voltage (prior to taking a map) to account for the CNP shift. This gate voltage is $\tilde{V}_g$. By using this procedure and applying the same sample bias voltage, the dI/dV maps in Figs 2c-e of the main text are configured to the same global charge density. This ensures differences seen between these maps arise primarily from changes in the local charge density profile.

2. Converting dI/dV intensity to charge density fluctuations after light-induced doping

The dI/dV maps in Figs 2c-e of the main text can be converted to charge density. In order to do this, we performed dI/dV measurements (with the STM feedback loop closed, V_s = -0.25 V, I = 0.2 nA) as a function of back-gate voltage V_g, an example of which is displayed in Fig. S1.

Here the conversion of dI/dV to charge density is relatively straightforward because the charge inhomogeneity δn induced by light exposure is small. Using Fig. S1 as a conversion tool, values of dI/dV in the line trace were matched to appropriate values of V_g. Finally, the line trace was converted to charge density through $|e|\delta n = C\,\delta V_g$, where C is capacitance per unit area calculated using a total SiO_2 and BN thickness of 360 nm (BN thickness measured by atomic force microscope).

3. Tip-doping dI/dV spectra with $V_g > 0$ V

Figure S3 shows four dI/dV spectra obtained on our graphene/BN heterostructure. Each spectrum was taken at $\tilde{V}_g = 0$ V and after an STM tip voltage pulse was applied while V_g was set to different positive values (in contrast to Fig. 3a of the main text, which shows the case for $V_g <$ 0 V). All the measurements were taken at the same location that the tip pulses were applied. The red curve is the original dI/dV spectrum obtained before tip pulsing. The graphene Dirac point (DP), which is denoted by the black arrow, shifts to greater positive V_s values with each successive voltage pulse ($V_g = +10$ V, $+20$ V, $+30$ V for the yellow, green, and blue traces, respectively). This indicates that the sample becomes more p-doped after each pulse with $V_g > 0$ V. We note that it is the value of V_g during a tip pulse that determines the amount of tip-doping (i.e. each sufficiently long tip pulse ($\Delta t > 30$ sec. – see Supporting Information Section 5) acts as an independent excitation unaffected by the previous tip-doping history).

4. Converting dI/dV intensity to charge density after tip-doping

Figure 3c of the main text can be converted to charge density through a similar method. The procedure for converting dI/dV to charge density is more complex here, however, because the charge density variation is not small and dI/dV is not monotonic with V_g over the range of interest. We summarize our conversion algorithm here (in more technical language, we use a combination of dynamic time warping with a Euclidean metric and locally weighted linear regression). First, Fig. 3c of the main text was radially averaged (the top right corner is the center point) to reduce the influence of the moiré superlattice and dot defects on the conversion algorithm. The radially averaged dI/dV was then matched to V_g values using a dI/d$V($V_g$) curve, ensuring that $V_g(r)$ is a continuous function of the radial distance r. The V_g values were then converted to charge density through $|e|\Delta n = C\,\Delta V_g$. We performed this algorithm on dI/dV maps

taken at the same location at different V_g set points, and the resulting charge density curves are in good agreement (with a constant offset corresponding to the different V_g set point). Figure S2a shows the result of this dI/dV-to-charge-density conversion. Applying the conversion algorithm to dI/dV maps with different V_s set points yields slight discrepancies (~ 10%), which we attribute to tip-induced band bending.

We can also apply this algorithm without radially averaging a dI/dV map (in this case we first smooth the map using linear interpolation to remove the moiré lattice). This yields a charge density map as shown in Fig. S2b. The charge density map shows only small deviations from circular symmetry, justifying the radial average used to construct the charge density profile in Fig. S2a.

5. Tip pulsing procedure

Here we present the procedure for creating a graphene pn junction through a tip pulse:

1. Set -1 V $\leq V_s \leq$ 1 V and $V_g = V_g^*$ under closed loop conditions, where V_g^* is the desired shift of the local charge neutrality point.

2. Open the STM feedback loop.

3. Withdraw the STM tip by $0.5 \leq \Delta z \leq 2.5$ nm. This tip pulse procedure also works in the tunneling regime (i.e. $\Delta z = 0$ nm), but can potentially damage the graphene or tip at such close distances.

4. Increase V_s to +5 V.

5. Wait Δt seconds. The wait-time Δt depends on the tip geometry and tip-sample distance, but needs to be significantly long to fully shift the local Dirac point E_D at $V_g = V_g^*$ to

$E_D(V_g = 0\ V)$. Usually, $\Delta t = 30$ sec. is sufficient for $\Delta z = 1$ nm (although Δt can be significantly shorter for $\Delta z < 1$ nm and longer for $\Delta z > 1$ nm).

6. Decrease V_s back to the original value.

7. Close the STM feedback loop.

8. Set $V_g = 0$ V. The Dirac point at $V_g = 0$ V is now at $E_D(V_g = -V_g{}^*)$ before the tip pulse procedure.

6. G(V_g) before and after tip-doping

G(V_g) measurements of a two-terminal device were acquired before and after tip-doping in order to explore the electronic functionality of our doping technique. These measurements were performed at ~77 K in our STM and are plotted in Fig. S4. The response of the device prior to tip-doping is shown as the red trace. Here a single dip in G(V_g) can be seen at $V_g \sim$ -22 V, which marks the CNP. We then set $V_g = 15$ V and performed tip pulses using our STM tip at 12 different locations within a 200 nm radius on the sample (see Supporting Information Section 5 for tip-doping procedure). The approximate location of the tip-doping array is depicted by the red "x" on the graphene flake in the inset of Fig. S4. The G(V_g) curve measured after the tip-doping is shown as the blue trace. Here we see a new, additional dip in G(V_g) located at $V_g \sim 15$ V. The existence of these two dips in G(V_g) indicates that a graphene pn junction was created using our tip-doping technique (such signatures have been observed in previous transport measurements of graphene pn junctions[1, 2]).

7. Nature of BN defects

For the high-purity single-crystal BN used in our study (synthesized by T. Taniguchi and K. Watanabe[3]), secondary ion mass spectroscopy identified oxygen and carbon impurities as prominent defect types[4]. Additionally, a comparison between recent optoelectronic experiments on BN crystals [5, 6] with theoretical work[7] shows that the nature of defects in these crystals is consistent with nitrogen vacancies and carbon impurities. Existence of the carbon impurities was further supported by recent STM studies on graphene/BN heterostructures[8]. Using the measured impurity density for bulk BN crystals from Taniguchi *et al.* [4], we estimate a defect density of ~10^{15} cm^{-2} for a 100 nm thick BN flake (distributed through the entire thickness).

Figure Captions:

Figure S1: dI/d$V(V_g)$ curve used for converting dI/dV to charge density. This dI/d$V(V_g)$ curve was taken after a short light exposure was imparted on the sample (20 seconds), while holding V_g = -15 V. Changes seen in dI/dV amplitude from Fig. 2d can be converted to charge density fluctuation by using the above measured dI/d$V(V_g)$ curve and $|e|\delta n = C \, \delta V_g$, in which C is capacitance per unit area.

Figure S2: Charge carrier density map obtained from a dI/dV map after an STM tip pulse. (a) Radially averaged $n(r)$ obtained from Fig. 3c of the main text using the procedure outlined in Supporting Information Section 3. (b) $n(x,y)$ is obtained by a similar procedure as (a). The map depicts a nanoscale pn junction that was created by an STM tip pulse.

Figure S3: Nanoscale doping controlled with an STM tip voltage pulse. (a) dI/dV spectroscopy of a pristine surface before a tip pulse (red) and after a tip pulse (V_s = 5 V, 30 sec.) for V_g = 10 V (yellow), 20 V (green), and 30 V (blue). Initial tunneling parameters: I = 0.4 nA, V_s = -0.5 V, $\tilde{V}_g$ = 0. The curves are vertically offset for clarity.

Figure S4: Tip-doped device transport data before and after tip-doping. Inset: Optical micrograph of device consisting of graphene (outlined by dashed lines) on an ~80nm thick BN flake (green) that is contacted by Cr/Au electrodes (yellow). Scale bar, 5 μm. G(V_g) curves obtained at ~77 K before tip-doping (red) and after tip-doping (blue). Tip-doping was performed at 12 different locations on an evenly spaced grid over a 4μm x 4μm area approximately centered at the red "x" seen in the inset (tip-doping parameters: V_s = 5V, 20 secs, V_g = 15V). The red

curve shows a single CNP before tip-doping at $V_g = $ -22V. After tip-doping two CNPs are clearly seen ($V_g = $ -22V and $V_g = $ 16V), indicating the presence of a pn junction after the tip-doping treatment. All data were acquired from a device with a 6 μm width and 8 μm source-drain separation.

References:

(1)   Huard, B.; Sulpizio, J. A.; Stander, N.; Todd, K.; Yang, B.; Goldhaber-Gordon, D. *Phys. Rev. Lett.* **2007,** 98, 236803.

(2)   Williams, J. R.; DiCarlo, L.; Marcus, C. M. *Science* **2007,** 317, 638-641.

(3)   Watanabe, K.; Taniguchi, T.; Kanda, H. *Nature Mater.* **2004,** 3, (6), 404-409.

(4)   Taniguchi, T.; Watanabe, K. *J. Cryst. Growth* **2007,** 303, (2), 525-529.

(5)   Ju, L.; Velasco Jr., J.; Huang, E.; Kahn, S.; Nosiglia, C.; Tsai, H.-Z.; Yang, W.; Taniguchi, T.; Watanabe, K.; Zhang, Y.; Zhang, G.; Crommie, M.; Zettl, A.; Wang, F. *Nat. Nanotechnol.* **2014,** 9, (5), 348-352.

(6)   Remes, Z.; Nesladek, M.; Haenen, K.; Watanabe, K.; Taniguchi, T. *Phys. Status Solidi A* **2005,** 202, (11), 2229-2233.

(7)   Attaccalite, C.; Bockstedte, M.; Marini, A.; Rubio, A.; Wirtz, L. *Phys. Rev. B* **2011,** 83, (14), 144115.

(8)   Wong, D.; Velasco Jr., J.; Ju, L.; Lee, J.; Kahn, S.; Tsai, H. Z.; Germany, C.; Taniguchi, T.; Watanabe, K.; Zettl, A.; Wang, F.; Crommie, M. F. *Nat. Nanotechnol.* **2015,** 10, (11), 949-953.
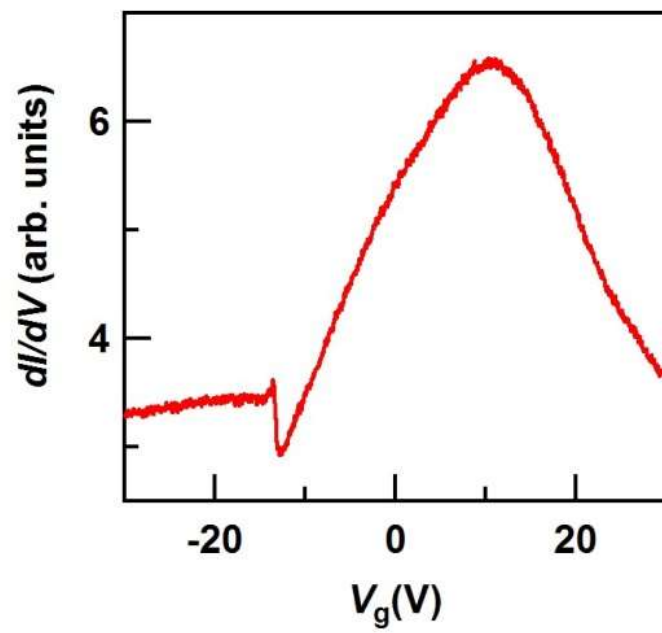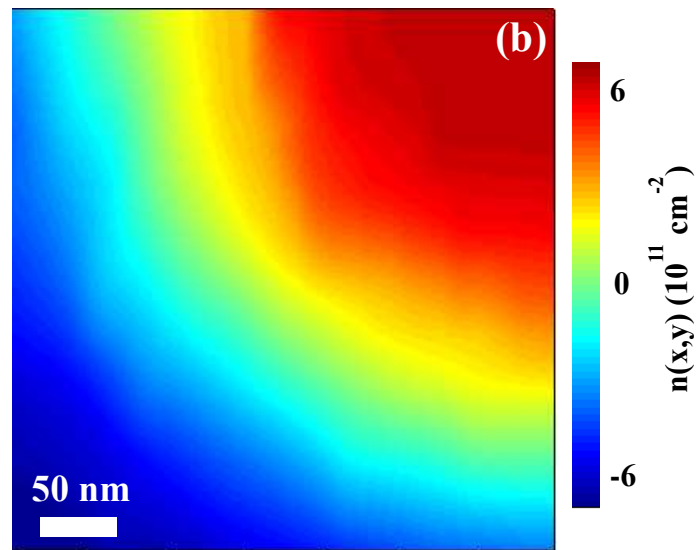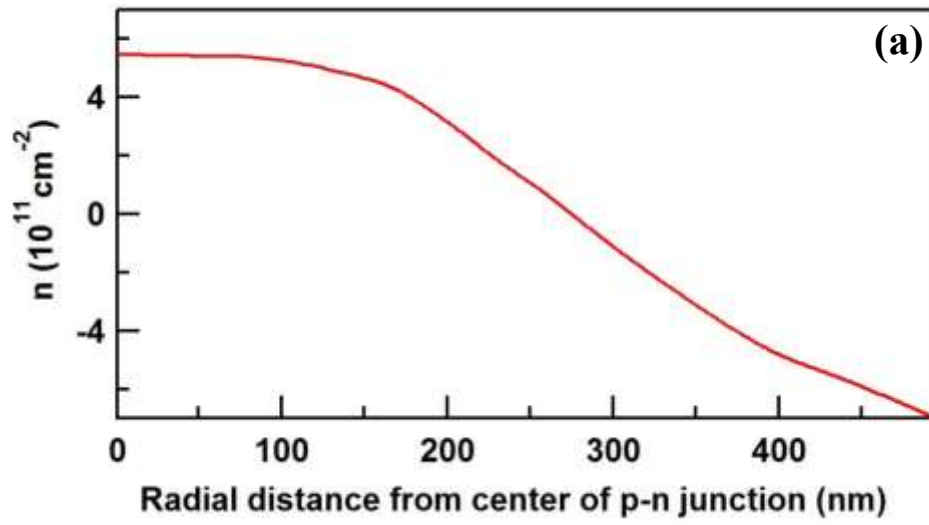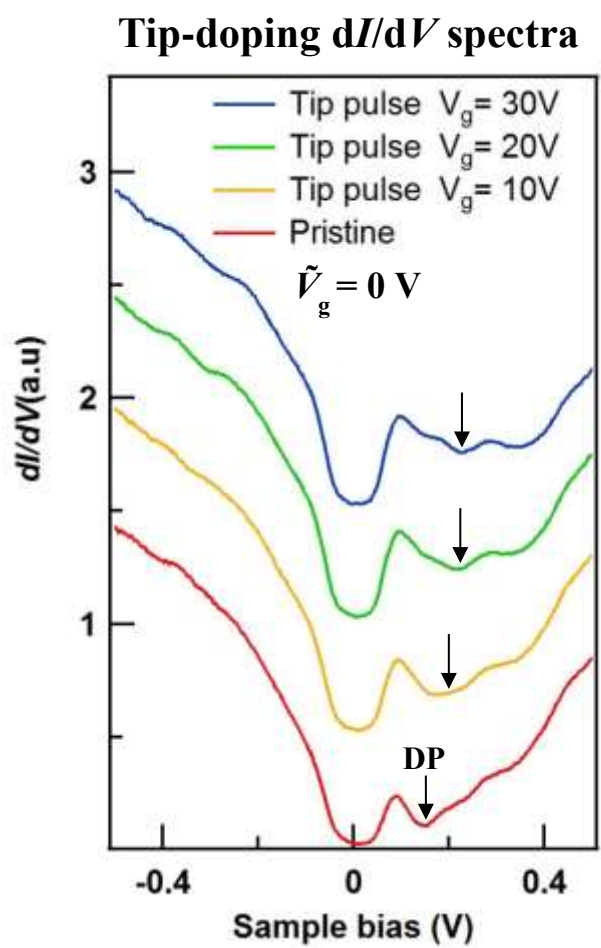
Figure S1

Figure S2

(a)

n $(10^{11}$ cm$^{-2})$

Radial distance from center of p-n junction (nm)

(b)

50 nm

n(x,y) $(10^{11}$ cm$^{-2})$

Figure S3

Tip-doping dI/dV spectra

Figure S4